Predin, Andrej; Klasinc, Roman; Biluš, Ignacijo

Cavitation Instabilities at the Entrance Pipe of Centrifugal Pump

Cavitation Instabilities at the Entrance Pipe of Centrifugal Pump

Andrej Predin[1], Roman Klasinc[2], Ignacijo Biluš[3]

ABSTRACT

The trend toward higher speed and power in order to achieve high performance characteristics has inevitably increased the potential for operating instabilities of modern pumps. Even in the absence of cavitation and its complications, these phenomena can lead to performance loss and in worst condition to structural failure.

One of the major sources of instability in a centrifugal pump is, as mentioned, cavitation within the pump. Cavitation of a centrifugal pump is the result of insufficient net positive suction head and can occur within the entire range of operating conditions. Cavitation may cause three different and undesirable effects: First - pump head and pump efficiency drop, second - impeller damage by pitting and erosion, and the third - structure vibration and resulting noise, [1]. Therefore, the cavitation process must be prevented by all means. Present contribution deals with influences of the simple motionless four blade guiding device on cavitating characteristics of radial pump.

In case of cavitating flow regimes; three distinct operating possibilities are known: First, the stable regime, where the majority of cavitating centrifugal pumps operate, Second, the unstable regime described as hydro dynamically induced cavitation surging, and the third - transient regime, described as thermodynamically induced surging, [2].

KEYWORDS:

Cavitation, pressure pulsations, casing vibrations, centrifugal pump, computational fluid dynamics, measurements

1. Introduction - Cavitation Surging

Hydro dynamically induced surging can occur at low values of capacity in almost all centrifugal pumps. The onset and intensity of cavitation surging is primarily determined by the shape of the impeller blades at impeller inlet. The extent to which cavities travel away from the impeller is determined by inlet pipe geometry. In most impeller – pipe configurations the low pressure regions are localised and backflow recirculation giving raise to cavitation surging hardly leaves the inlet blade region. In some pumps however, particularly those for which the inlet pipe has axial symmetry with impeller eye, the associated backflow extends well into the inlet pipe. It is known, that in pumps, where a backflow recirculation device (Figure 1.b) is fitted, the intensity and extent of surging is much reduced over a wide flowrate range.

[1] Prof. dr. Andrej PREDIN, University of Maribor, Faculty of Mechanical Engineering, Smetanova ulica 17, Maribor, Slovenia, e-mail: Andrej.Predin@uni-mb.si
[2] Prof. dr. Roman KLASINC, Institute for Hydraulic Resources and Water Management, Graz Technology University, Stremayrgasse 10/II, A- 8010 Graz AUSTRIA, e-mail: Roman.Klasinc@TUGraz.at
[3] Dr. Ignacijo BILUŠ, University of Maribor, Faculty of Mechanical Engineering, Smetanova ulica 17, Maribor, Slovenia, e-mail: Ignacijo.Bilus@uni-mb.si

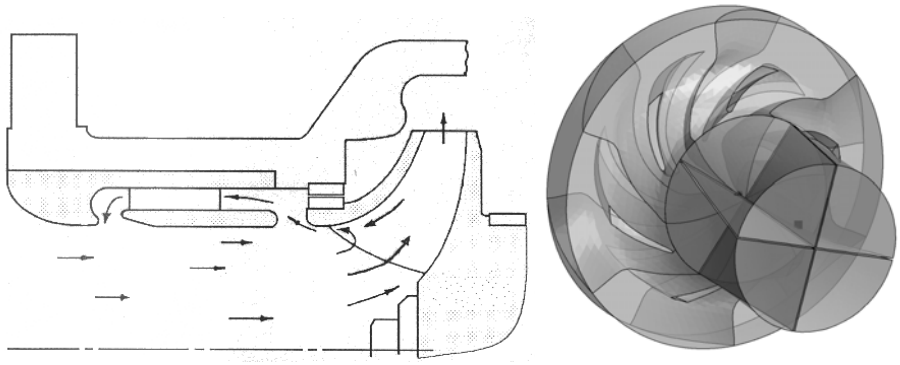

a) b)

Figure 1: Backflow recirculation system (a) and simple axial flow guiding device in front of centrifugal impeller (b)

Another known powerful method to improve the cavitation performance is the attachment of an inducer just upstream of the main impeller [4] and many researchers all over the world study different pump inducer geometry versions in order to achieve reliable and cavitation free operating characteristics [4], [5].
According to relative complicated "pipe in pipe" construction of backflow recirculation system and regarding to pump inducer price, the simplified flow guiding device, shown in figure 1, was used for cavitation surging decrease. The main advantage of presented system should be in simple design and low price.

1.1 Physical model geometry

Simple copper made cross in form of 4 guiding blades with inclination angle α=20º was put into the transparent pipe at the impeller entrance. Guiding blades length was equal $l = 1.15 \cdot D$, where D present the inlet pipe diameter.
Described flow guiding pipe system was connected to the conventional closed loop pump testing installation as shown in figure2.

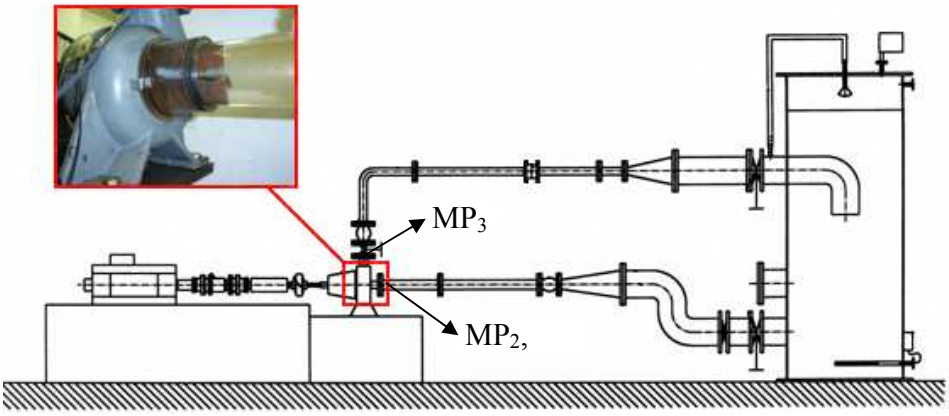

Figure 2: Measuring system drawing

For test purposes, commercial radial water pump with design speed 2900 rpm, maximal capacity $Q_{\max} = 0.027\,\mathrm{m}^3/\mathrm{s}$ and maximal head $H_{\max} = 25\,\mathrm{m}$ was used. Operating characteristics of the pump are evident from figure 3 (a).

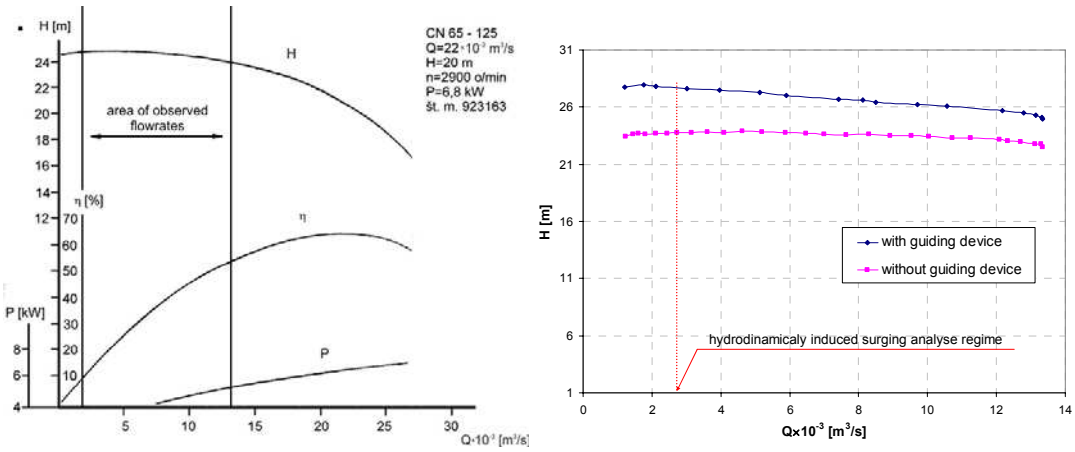

a) **b)**

Figure 3: Operating characteristics of tested pump (a) and measured influence of guiding device on pressure difference curve (b)

It is evident from the figure 3 (b) that measured pressure difference curve agrees with operating characteristic defined by the pump manufacturer figure 3 (a) in the case of conventional inlet pipe geometry. On the other side, it is also evident that guiding vanes device increases the achieved pressure difference at the flow rates up to $Q = 0.5 \cdot Q_{\max}$. The reason for this could be found in better flow attack angles at the pump inlet.

2 Cavitation surge pressure pulsations

Pressure pulsations connected to cavitation surging were measured at the three different measuring points placed in the upstream (MP_2, MP_1) and downstream (MP_3) direction of radial pump entrance pipe as shown in figure 2.
Absolute piezo – resistive pressure transducers KELLER with pressure range up to 2 and up to 10 bar (FS) with frequency response 20 kHz were connected to A/D measuring equipment. Pressure pulsations were analysed at different NPSH values of pump installation at flowrate equal to 12% of flowrate at best efficiency point (Q_{BEP}).

2.1 Measurements results

Normalised autocorrelation record of pressure distribution function was performed in order to show the periodic nature of the phenomenon. Figure shows the results for different measuring points (MP_2 at $3 \cdot D$ and MP_1 at distance equal to $5 \cdot D$ from impeller eye).

Good correlation is evident from figure 4, since function values lie in the range from 0.991 up to 0.997. According to this, frequency analyses with Fast Fourier transformation (FFT) was made for two different values of pressure in water reservoir and different NPSH, respectively. Same operating regime was set for the example with and without guiding device. Frequency analyses results records are shown in plots at figure 5 up to 9 at, a) Higher NPSH and, at figure 9,b) Lower NPSH.

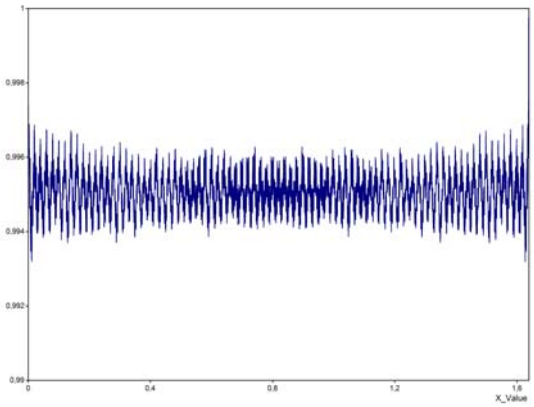

a) MP1 at higher NPSH

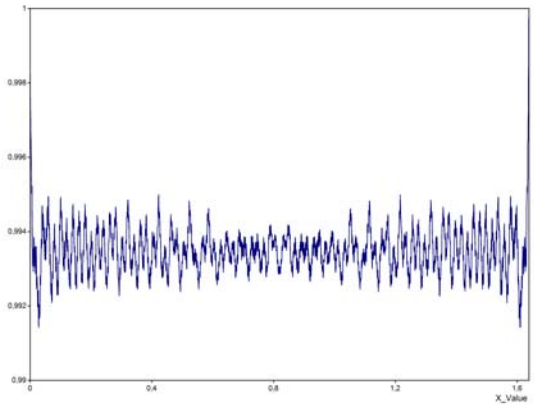

b) MP2 at higher NPSH

Figure 4: Normalized autocorrelation of pressure distribution functions

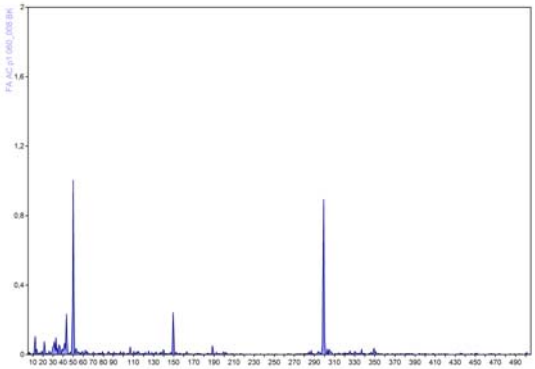

Figure5: Pressure pulsations at MP_1 without guiding blades and higher NPSH value

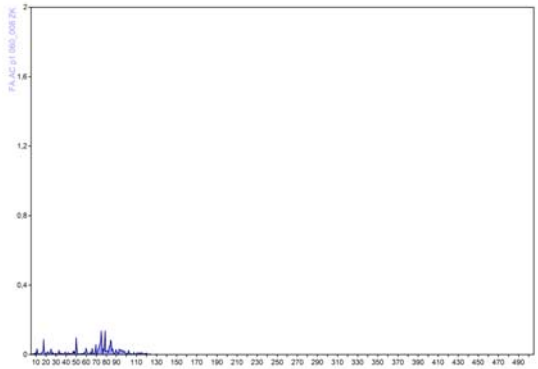

Figure6: Pressure pulsations at MP_1 with guiding blades and higher NPSH value

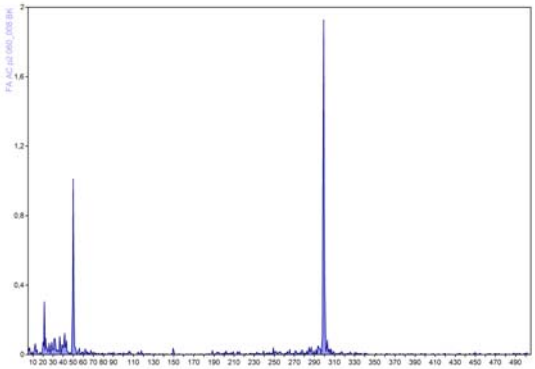

Figure7: Pressure pulsations at MP_2 without guiding blades and higher NPSH value

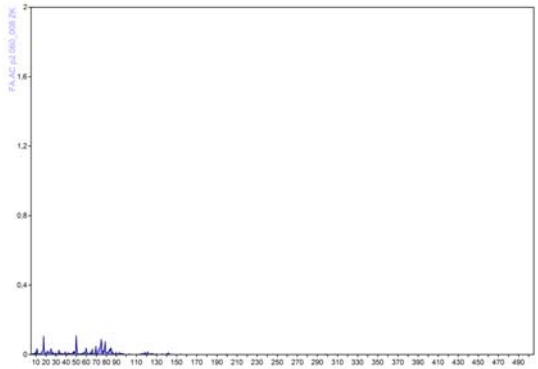

Figure 8: Pressure pulsations at MP_2 with guiding blades and higher NPSH value

It is evident from frequency analyses presented in figure 5 and figure 6, that guiding blades reduce the amplitudes at whole frequency range. This amplitude chocking is especially strong at rotating impeller basic frequency $f_{imp} \approx 50\ Hz$, its harmonics and blade passing frequency $f_{blade} \approx 300\ Hz$ with its sub-harmonic.

These results confirm other authors' analyses defining the super synchronous speeds of rotating cavitation with range up to 1.4 comparing to impeller rotating speed [6].

Following the relative strong pressure pulsations at distance equal to five pipe diameters ($5 \cdot D$) from impeller entrance eye, second measurement series were done at position MP_2 corresponding to distance equal to three inlet pipe diameters ($3 \cdot D$).

From the presented FFT analyse of pressure pulsations at MP_2 could be concluded that the guiding device reduces pressure pulsation amplitudes of characteristic frequencies and hydro dynamically induced surge pulsations with lower frequencies [2].
According to the distance dependency of pulsation measurements, additional results comparison was made analysing the influence of pressure values (NPSH) on pulsations. Figure 9 shows pressure pulsations at MP_1 and different values of NPSH.

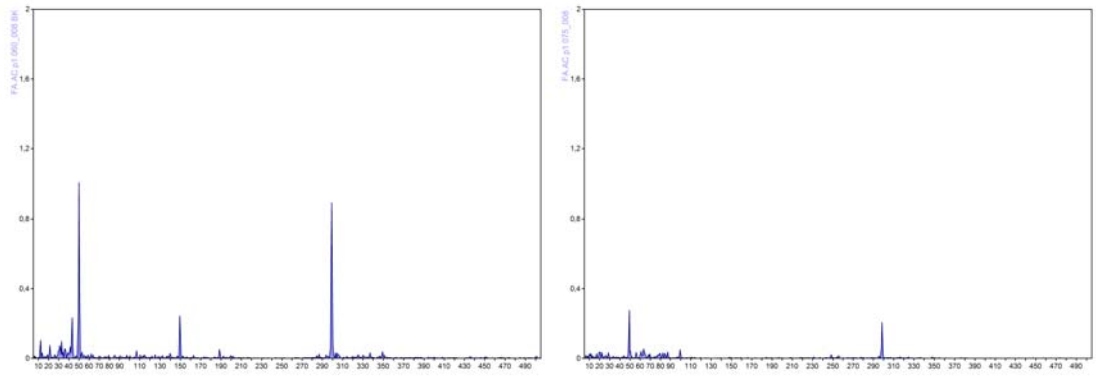

a) Higher NPSH **b) Lower NPSH**

Figure 9: Pressure pulsations at MP_1 and different NPSH values without guiding blades

Pressure level decrease reduces the amplitudes of pulsations at the whole frequency range is evident at figure 9. The reason for this could be in the interaction of the complicated surge mechanisms with intensified rotating cavitation [6].

3 Numerical simulation

Owing to fast computer capabilities increase and according to intensive measurement methods development, numerical simulation of cavitating (multiphase) flows became possible in the past years.

Considering of homogenous flow, common flow field and other relevant fields such as temperature and turbulence are shared by both fluids (water and water vapour). This allows some simplifications to be made to the multi fluid model. For a given transport process, the homogenous model assumes that the transport quantities (with the exception of volume fraction) for that process are the same for both phases.
Homogenous two phase transport model included in commercial software ANSYS-CFX was used for surging simulation.

The Rayleigh Plesset model is implemented in the multiphase framework as an interphase mass transfer model in used numerical code. The Rayleigh-Plesset equation provides the basis for the rate equation controlling vapour generation and condensation. The Rayleigh-Plesset equation describing the growth of a gas bubble in a liquid is given by:

$$R_B = \frac{d^2 R_B}{dt^2} + \frac{3}{2}\left(\frac{dR_B}{dt}\right)^2 + \frac{2\sigma}{\rho_f R_B} = \frac{p_v - p}{\rho_f} \qquad (1)$$

where R_B represents the bubble radius, p_v is the pressure in the bubble (assumed to be the vapour pressure at the liquid temperature), p is the pressure in the liquid surrounding the bubble, ρ_f is the liquid density, and σ is the surface tension coefficient between the liquid and vapour. Note that this is derived from a mechanical balance, assuming no thermal barriers to bubble growth. Neglecting the second order terms (which is appropriate for low oscillation frequencies) and the surface tension, this equation reduces to:

$$\frac{dR_B}{dt} = \sqrt{\frac{2}{3}\frac{p_v - p}{\rho_f}} \tag{2}$$

The rate of change of bubble volume follows as:

$$\frac{dV_B}{dt} = \frac{d}{dt}\left(\frac{4}{3}\pi v R_B^3\right) = 4\pi R_B^2 \sqrt{\frac{2}{3}\frac{p_v - p}{\rho_f}} \tag{3}$$

and the rate of change of bubble mass is:

$$\frac{dm_B}{dt} = \rho_g \frac{dV_B}{dt} = 4\pi R_B^2 \rho_g \sqrt{\frac{2}{3}\frac{p_v - p}{\rho_f}} \tag{4}$$

If there are N_B bubbles per unit volume, the volume fraction r_g may be expressed as:

$$r_g = V_B N_B = \frac{4}{3}\pi R_B^3 N_B \tag{5}$$

and the total interphase mass transfer rate per unit volume is:

$$\dot{m}_{fg} = N_B \frac{dm_B}{dt} = \frac{3 r_g \rho_g}{R_B} \sqrt{\frac{2}{3}\frac{p_v - p}{\rho_f}} \tag{6}$$

This expression has been derived assuming bubble growth (vaporization). It can be generalized to include condensation as follows:

$$\dot{m}_{fg} = F \frac{3 r_g \rho_g}{R_B} \sqrt{\frac{2}{3}\frac{|p_v - p|}{\rho_f}} \operatorname{sgn}(p_v - p) \tag{7}$$

where F is an empirical factor which may differ for condensation and vaporization, designed to account for the fact that they may occur at different rates (condensation is usually much slower than vaporization). Despite the fact that upper equation has been generalized for vaporization and condensation, it requires further modification in the case of vaporization. Vaporization is initiated at nucleation sites (most commonly non-condensible gases). As the vapor volume fraction increases, the nucleation site density must decrease accordingly, since there is less liquid. For vaporization, r_g is replaced by $r_{nuc}(1 - r_g)$ to give:

$$\dot{m}_{fg} = F \frac{3 r_{nuc}(1 - r_g)\rho_g}{R_B} \sqrt{\frac{2}{3}\frac{|p_v - p|}{\rho_f}} \operatorname{sgn}(p_v - p) \tag{8}$$

where r_{nuc} is the volume fraction of the nucleation sites. Source equation is maintained in the case of condensation. It is important to note that in this model R_B represents the radius of the nucleation sites.

To obtain an interphase mass transfer rate, further assumptions regarding the bubble concentration and radius are required. The Rayleigh Plesset cavitation model implemented in ANSYS CFX uses the following defaults for the model parameters:
$R_B = 1\mu m$, $r_{nuc} = 5 \times 10^{-4}$, $F_{vap} = 50$, $F_{cond} = 0.01$.

3.1 CFD results

The present chapter includes results comparison for both inlet pipe geometries (with and without guiding device). Diagrams and photographs are showing same operating regime regarding relative pressure in the water reservoir (NPSH value) and convection term (flowrate) height. The influence of geometry on cavitation swirl has been analysed with stress laid on two phase area propagation.
Since we have to model a change in a reference frame between the rotating domain (impeller) and stationary domain (pipe), the transient fluid – fluid interface has been defined. At the figure 10, a) and b), is visible the operating regime pattern for system operating out of design point – with reduced flowrate for both geometries.

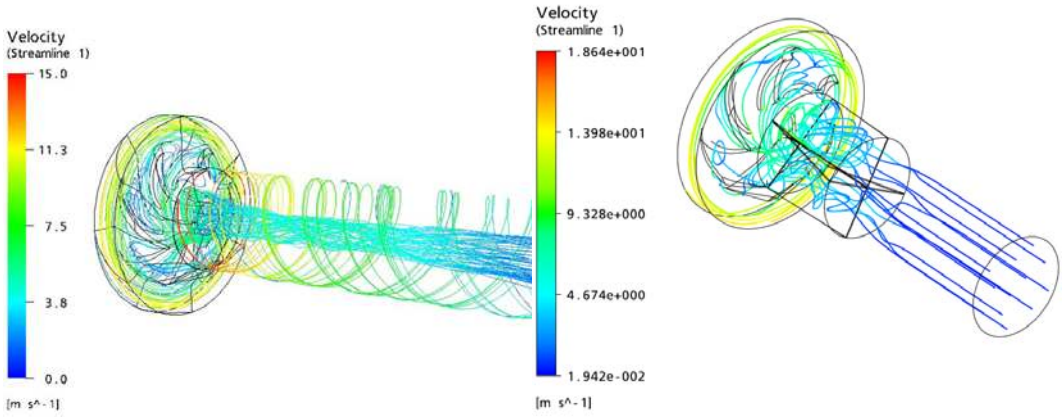

a) **b)**

Figure 1: Operating regime visualization using streamlines plots for both analysed geometries

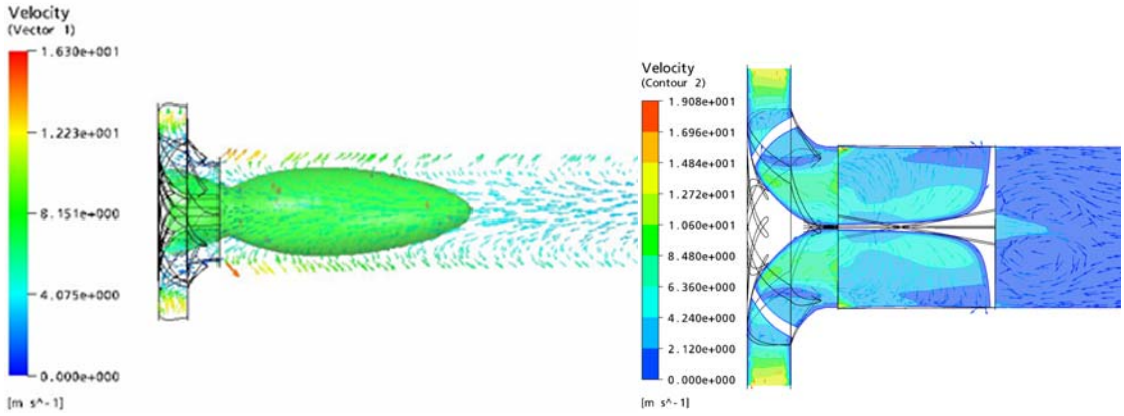

a) **b)**

Figure 2: Unstable cavitating pump operating regime

Strong prerotating motion [7] in the inlet pipe especially near pipe walls is evident from the figure 10 (a) showing the case of geometry without guiding device.
Comparing to the streamlines plot at figure 10 (b) it could be concluded, that guiding device stops general swirling flow and splits it into four smaller flow channels where smaller swirls occur. Pictures (Figure 11) shows the unstable cavitating operating regime with a strong recirculating cloud of vapour bubbles at the inlet pipe walls connected to cavitation number decrease.

Strong recirculatory motion with an active flow area in the middle of the pump is shown in the picture showing geometry without guiding device, figure 12 (a). It is obvious from water vapor isosurface that cavitation swirl takes place in the low pressure region of the active flow area.

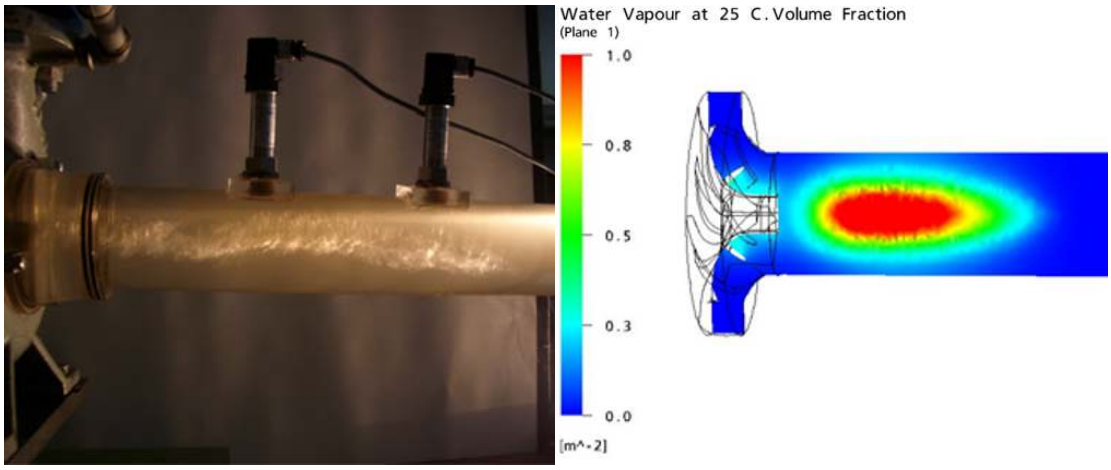

a) **b)**

Figure 12: Hydro dynamically induced Cavitation Surging on the inlet geometry without guiding device

Splitted recirculation cloud is evident from figure 13 (a). Figure 13 (b) shows operating regime with guiding device, where cavitation cloud remains in the guiding device channels.

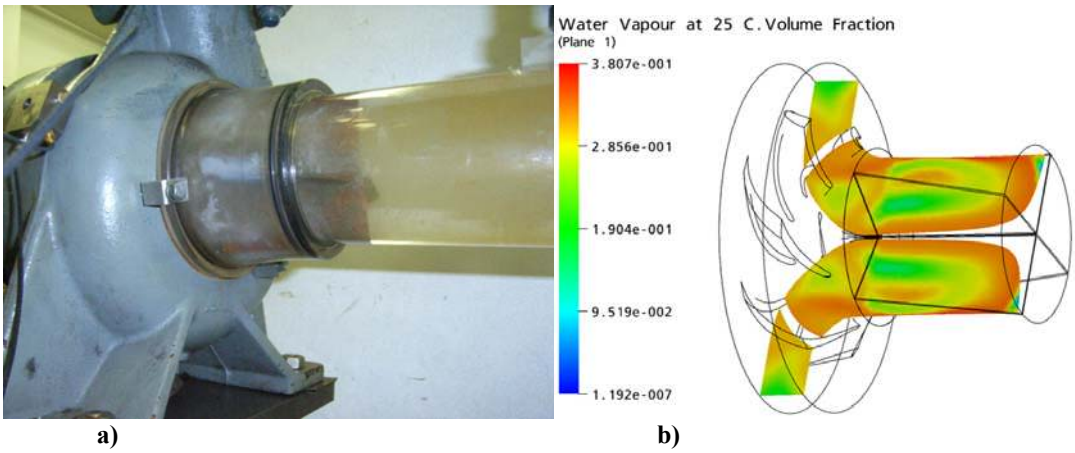

a) **b)**

Figure 13: Hydro dynamically induced Cavitation Surging on inlet geometry with guiding device

Figure 12 (b) and 13 (b) shows the cavitation visualization comparison at both intake pipe geometries.

From figures 12 and 13 it can be concluded that guiding vanes split the rotating two phase region into the four flow passages. Evident is that the cavitation region becomes shorter.
Based on good agreement, evident on photo comparing to CFD simulation results, it could be finalized, that used homogenous cavitation transport model based on the Raleigh – Plesset equation (as inter phase mass transfer model) presents effective tool for cavitation prediction in hydraulic machinery.

4 Mathematical models for frequency analysis

Apart from the fact that computer performances increased rapidly in past years, we are still not able to make full frequency analysis using computational fluid mechanics results. The reason for this could be found in the limited computer memory and calculation times. According to this, multi frequency instabilities of cavitating turbo machinery parts (especially for multi-blade impellers) can be analyzed using different analytical models. Recent investigations of cavitating turbopump inducers [8] has revealed the existence of more complex instabilities then previously recognised cavitation surge and rotating cavitation. These multifrequency instabilities were not under scope of present study and can be find also in relevant literature [6] and [9].

5 Conclusions

Hydro dynamically induced surge is system instability that involves not just the pump characteristics but those of the complete piping system at complicated unstable operating regime. Present contribution presents the experimental and numerical analyses approach. Results show that use of the simple guiding device results in dominant pressure pulsations and cavitation region decrease.
It is evident from the experimental analysis that dominant frequencies scale with the impeller rotating speeds, where some of them show large independency of the impeller rotation frequency at both inlet pipe geometries.
It can be written that used homogenous mathematical model for cavitation presents suitable tool for prediction of cavitation in turbo machinery and fast method for geometry influence analysis.
The computational fluid mechanics results show that the cavitation region transition from the area of impeller channels up in the entrance pipe is connected to recirculation flow and with decreased active flow area in the intake pipe respectively.
The swirl length is based on the geometry of the pump entrance area and pressure in the reservoir, which defines the volume fraction of the gas phase and the cavitation swirl diameter.
Simple guiding device splits the prerotating flow motion into four disconnected flow channels resulting in operating characteristics increase and possible operating complications connected with pressure pulsations and vibrations decrease.
Owing to transient nature of complicated turbulent two phase flow regime in analysed system, both numerical and experimental research methods should be used.

6 References

[1] M. Čudina, 2006, Noise as an indicator of cavitation in a centrifugal pump, Acoustical Physics, Volume 49, Number 4. http://www.springerlink.com/content/y2752m7ju272l375

[2] A. Bergant, 2000, Transient cavitating flow in piping systems. *Acta hydrotech.*, Volume 18, Number 29.

[3] Edward Grist, 1998, Cavitation and the Centrifugal Pump, A Guide for Pump Users, Taylor and Francis, London.

[4] T. Kimura, 2006, Numerical Simulation for Unsteady Cavitating Flow in a TurboPump Inducer, International Symposium on Cavitation, CAV 2006, Wageningen, Netherlands.

[5] J.H. Kim, 2006, Suppression of Cavitation Surge of Impeller Inducer by Inserting Ring – shaped Inlet Plate, International Symposium on Cavitation, CAV 2006, Wageningen, Netherlands.

[6] C.E: Brennen, 1994, Hydrodynamics of Pumps, Concepts ETI Inc, USA and Oxford University Press, England.

[7] A. Predin, 2003, Influence of additional inlet flow on the prerotation and performance of centrifugal impellers, Journal of Hydraulic Research, Volume 41, Number 2.

[8] C.E. Brennen, 2006, A Multifrequency Instability of Cavitating Inducers, International Symposium on Cavitation, CAV 2006, Wageningen, Netherlands.

[9] International Symposium on Cavitation, Cav 2006, 11 – 15 September 2006, Wageningen, Netherlands, http://www.cav2006.com

7 Notations

R_B bubble radius,

p_v pressure in the bubble,

p pressure in the surrounding liquid,

ρ_f liquid density,

ρ_g vapour density,

σ surface tension between the liquid and vapour,

V_B bubble volume,

m_B bubble mass,

t time,

N_B bubble number density,

r_g volume fraction,

$\dot{m}_{fg}$ interphase mass transfer per unit volume,

F empirical factor,

r_{nuc} volume fraction of nucleation sites